RESEARCH ARTICLE | JANUARY 17 2024

Proton doping enhanced flexoelectricity and photocurrent in hydrogen-charged TiO_2

Z. L. Wang ; Yangshi Jin ; Chun Hung Suen ; Chenyue Mao; Xiangnan Gong ; Jiangping Ma; J. W. Hong ; F. Zhang ; Chi-Ho Wong ; W. P. Chen ; X. Y. Zhou ; Ji-Yan Dai

Appl. Phys. Lett. 124, 032902 (2024)
https://doi.org/10.1063/5.0180626

Applied Physics Letters ARTICLE pubs.aip.org/aip/apl

Proton doping enhanced flexoelectricity and photocurrent in hydrogen-charged TiO_2

Cite as: Appl. Phys. Lett. **124**, 032902 (2024); doi: 10.1063/5.0180626
Submitted: 11 October 2023 · Accepted: 1 January 2024 ·
Published Online: 17 January 2024

Z. L. Wang,[1] Yangshi Jin,[1] Chun Hung Suen,[1] Chenyue Mao,[2] Xiangnan Gong,[3] Jiangping Ma,[3] J. W. Hong,[4] F. Zhang,[5] Chi-Ho Wong,[6,a)] W. P. Chen,[2,a)] X. Y. Zhou,[3,a)] and Ji-Yan Dai[1,a)]

AFFILIATIONS

[1]Department of Applied Physics, The Hong Kong Polytechnic University, Hong Kong 999077, China
[2]Department of Physics, Wuhan University, Wuhan 430072, China
[3]College of Physics, Chongqing University, Chongqing 401331, China
[4]School of Aerospace Engineering, Beijing Institute of Technology, Beijing 100081, China
[5]State Key Laboratory of Information Photonics and Optical Communications & School of Science, Beijing University of Posts and Telecommunications, Beijing 100876, China
[6]Department of Physics, The Hong Kong University of Science and Technology, Hong Kong 999077, China

[a)]**Authors to whom correspondence should be addressed:** jiyan.dai@polyu.edu.hk; wpchen@whu.edu.cn; xiaoyuan2013@cqu.edu.cn; and chkhwong@ust.hk

ABSTRACT

The intrinsic flexoelectric effect observed in oxide materials often falls below the desired threshold for practical applications. In this work, we demonstrate proton doping in insulating rutile TiO_2 crystal as an effective approach to significantly increase flexoelectricity by more than two orders of magnitude. We attribute the noteworthy enhancement of flexoelectricity to the dual impact of proton doping in oxide materials. First, proton doping serves to induce the presence of charge carriers, resulting in the generation of flexoelectric currents. Second, proton doping induces expansion and distortion of the lattice structure, leading to an amplified flexoelectric field when the crystal experiences a strain gradient. The formation of O–H bonding in TiO_2 crystal provides another route to break centrosymmetry according to lattice distortion of the TiO_2 lattice, resulting in a larger flexoelectric field. In addition, the introduction of proton doping in TiO_2 single crystals leads to a substantial increase in photocurrent by effectively flattening the interfacial Schottky junction. This phenomenon results in a three-order of magnitude enhancement of the photocurrent. Our work broadens the horizon of study on dielectric materials through proton doping and may also provide an approach that enables the utilization of dielectric materials in energy conversion applications.

Flexoelectricity describes electric polarization of materials in response to strain gradient, and this effect has the potential for a wide range of applications in many aspects.[1–5] To enhance the generally small flexoelectricity toward application, many recent studies have largely expanded the flexoelectric effects from a simple polarization concept to a modulation strategy in a wide range of functional materials.[6–11] Enhanced flexoelectricity has been demonstrated in oxide perovskite materials such as (Ba,Sr)TiO_3 ceramics through approaches like doping-induced charge carriers and space inversion symmetry breaking induced electric polarization.[12–14] Yang *et al.* also raised the idea of the flexo-photovoltaic (PV) effect, where the strain gradient-induced polarization in centrosymmetric materials could induce the PV effect analogous to the ferroelectric PV effect.[2] Later on, Shu *et al.* discovered that ultraviolet light (UV) can enhance the flexoelectricity by two orders of magnitude for hybrid perovskites, and they further proved that such photo-flexoelectricity can be a general property of semiconductors.[15] Motivated by the fact that oxygen vacancy density in materials can influence their flexoelectric property, a three-order-of-magnitude larger flexoelectric coefficient has been reported in $LaAlO_3$/$SrTiO_3$ interfaces.[10,16,17] Our previous work also demonstrated one order of magnitude enhancement and strong photo-flexoelectric effect by vacuum annealing induced Ti ion degradation and charge carriers in $SrTiO_3$ single crystals.[18] In addition to these flexoelectric effects of perovskite oxides,[19,20] recent studies have also discovered some interesting mechanical properties arising from the interaction between the piezoelectric effect and the flexoelectric effect.[21–24] These properties imply that the mechanical response can be modulated by strain gradient,[25,26] and the large strain gradient at small scales can also be directly

observed by scanning transmission electron microscopy.[27,28] In addition to conventional force-electric coupling effects through strain gradients designed to model energy harvesters,[29–34] memory,[35] sensors,[36] and actuators,[37,38] flexoelectric effect can also be related to many other important physical behaviors.[39] For example, it has been found that, as a result of flexoelectricity, transverse shear surface acoustic waves are able to propagate close to the smooth outer layer belonging to each crystalline dielectric.[40] More applications of flexoelectric effect include domain tailoring and polarization switching, in which mechanical deformation gradients may modify the spontaneous polarization state of nanoscale materials;[41,42] these powerful features are attracting increased attention.

Recently, the reactions between hydrogen and metal oxide materials have drawn significant attention.[43–45] Incorporating hydrogen (or proton doping) is a common technique used to increase charge concentration in oxide materials. This leads to a decrease in resistance,[46–48] but it also results in increased dielectric loss.[49] For instance, hydrogen-charged anatase TiO_2 crystals in nanoscale have tremendously enhanced photocatalytic performances, as reported by Chen *et al.*[50] Furthermore, hydrogen-charged TiO_2 nanocrystal arrays exhibited excellent photoelectrochemical performance through water electrolysis.[51] However, the proposed mechanisms for the aforementioned behaviors diverge in different research. The reduction of the bandgap of TiO_2 is mainly attributed to the interstitial proton,[52,53] rather than surface disorders.[48,54,55]

The coupling between flexoelectricity and doping, as one of the most promising phenomena from a practical point of view, has triggered numerous investigations and discussions in the flexoelectricity-related research community.[14,50,56–58] The use of oxygen vacancies induced by high-temperature annealing can enhance the flexoelectricity of $SrTiO_3$,[18,59] and we expect that proton doping can make the flexoelectricity of metal oxides more robust. Beyond that, the dynamics of proton driven by flexoelectric field may also enhance the effective flexoelectricity. Hence, studying the flexoelectricity in oxide single crystals with respect to charge concentration could be a promising approach. The formation of O–H bonding also provides another degree of freedom to break centrosymmetry, giving rise to flexoelectricity; therefore, a large flexoelectric response could be achieved in the TiO_2 crystal. In this work, the flexoelectricity of pristine and proton doped TiO_2 single crystals and their response to a bias voltage are compared, and coupling between the flexoelectric field and photocurrent as well as charge carriers is studied.

The TiO_2 single crystals used in this work were sourced from MTI Corporation. These crystals were two-sided polished and had a thickness of 0.5 mm. The bare crystal was then cut into beam shapes with a size of $7 \times 10\,mm^2$. To make the hydrogen-charged samples, polished rutile (001) single crystals were coated with an annealed silver electrode at a corner of the sample as cathode and then immersed in a 0.01M NaOH water solution for 168 h with 4.5 V voltage applied between the sample cathode and Pt anode electrode. Semi-transparent gold electrodes of 5 nm thick were sputter deposited on the two surfaces of the TiO_2 plates forming a capacitor structure (electrode/TiO_2/electrode). To measure the flexoelectricity, the free end of a clamped cantilever-shaped crystal was subjected to an oscillatory bending force delivered by a piezoelectric actuator. The induced alternating current, resulting from the oscillatory bending, was measured using a lock-in amplifier, which was connected to the electrodes through coaxial cables. Using standard elastic deformation equations, the strain gradient was calculated for a point-loaded single-clamped beam. This calculation takes into account the deflection amplitude and the distance from the clamped side and actuator contact point. The polarization was extracted from the amplitude of the oscillating current and the frequency of the actuator. The linear proportionality constant between polarization and strain gradient is called the flexoelectric coefficient. A PERKIN ELMER_UV-vis-NIR spectrometer was used to characterize the absorption spectra of the pristine and proton-charged TiO_2 crystal samples.

As shown in Figs. 1(a) and 1(b), the light absorption spectra of the pristine and hydrogen-charged TiO_2 samples were measured to determine the optimal wavelength range for photo-enhanced flexoelectricity. It is apparent that the hydrogen-charged TiO_2 crystal absorbs light more effective than the pristine TiO_2, and both samples show strong absorption to UV light below 365 nm wavelength. A UV laser with a 365 nm wavelength was suitable to induce the photovoltaic effect. To confirm the existence of protons in TiO_2, we conducted Fourier Transform Infrared (FTIR) characterization of the proton doped TiO_2 sample. As shown in Fig. 1(b), the absorption peak located at around $3280\,cm^{-1}$ wavenumbers indicates the formation of O–H bond, which can be a sign of proton identification.[60] The hydrogen-charged TiO_2 crystal becomes blue color but still transparent, also indicating the formation of O–H bond in the TiO_2 crystal, i.e., effective doping of protons. Proton doping also results in lattice expansion and distortion, which can be illustrated by the left shift of TiO_2 (002)

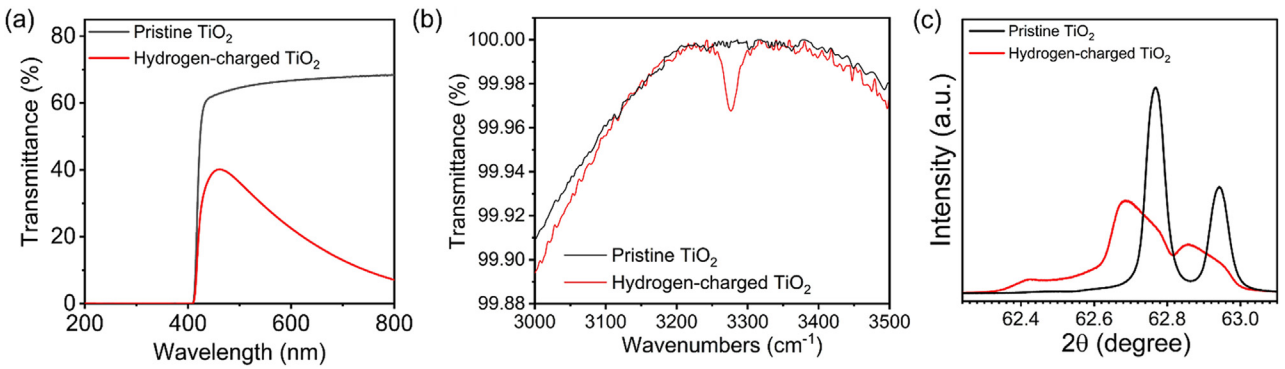

FIG. 1. Optical transmission spectra (a), FTIR spectra showing the absorption by O–H bonding (b), and XRD (002) peak (c) of pristine and proton doped TiO_2 crystals.

diffraction peak in XRD pattern shown in Fig. 1(c), where one can see clearly left shift of the peak for the hydrogen-charged sample.

The effective flexoelectric coefficients of the (001) TiO_2 single crystals with semi-transparent Au electrodes on both sides were measured with a setup shown in Fig. 2(a). With the generated flexoelectric current shown in Fig. 2(b), the polarizations under different strain gradients can be extracted and are shown in Fig. 2(c), where the labeled flexoelectric coefficients are calculated from the slope of the fitting lines. As depicted in Fig. 2(c), the u-shape bending of the pristine TiO_2 crystal reveals an effective flexoelectric coefficient of approximately 1 nC/m in the dark conditions. By contrast, the flexoelectric coefficient of the proton doped TiO_2 sample exhibits a significant enhancement exceeding two orders of magnitude. The effective flexoelectric coefficients of the hydrogen-charged TiO_2 crystal corresponding to the n- and u-shaped bending were also measured, and results are illustrated in Fig. 2(d). It is apparent that the sample is macroscopically symmetric for the top and bottom surfaces, and there is no obvious difference between the two bending modes in terms of the flexoelectric effect.

To further demonstrate the presence of charge carriers in the proton doped TiO_2, the photocurrent at the Au/TiO_2 interface was measured, and the results are shown in Figs. 3(a) and 3(b). One can observe that when UV light is incident on the top surface, it results in the photovoltaic effect and leads to the generation of photocurrent. It is intriguing to observe, as depicted in Fig. 3(b), that the photocurrent of the proton doped TiO_2 crystal is three orders of magnitude higher than that of the pristine crystal sample.

It should be noticed that the photocurrent is a persistently decayed current under constant UV light and does contribute to the alternative flexoelectric current, as measured by the lock-in amplifier. However, as illustrated in Figs. 3(c) and 3(d), incident light-induced electrons and holes can migrate to the electrodes, giving rise to enhanced photocurrent, i.e., the photovoltaic effect. Despite bending the sample, we did not observe significant increase in the photovoltaic effect, since compared to the large photocurrent, bending induced flexoelectric current is not obvious.

To further understand the proton doping effect in the crystal, the proton doped TiO_2 crystal was tested with I–V curve measurement by applying sweeping voltages from −10 to 10 V. As shown in Fig. 4(a), the sequence of the voltage sweeping is from 0 V to a maximum of positive voltage 10 V and then to a maximum of negative voltage −10 V, and finally back to 0 V. One can observe a hysteresis loop for proton doped TiO_2 in contrast to the pristine TiO_2 crystal. This indicates that protons in the crystal can migrate driven by the external electric field. The modulation of interfacial Schottky barriers generated by the proton migration can further trigger the switching between the high-resistance state (HRS) and the low-resistance state (LRS), which is similar to the reported switchable diode-type resistive switching behavior.[61,62] This resistive change caused by proton doping may be

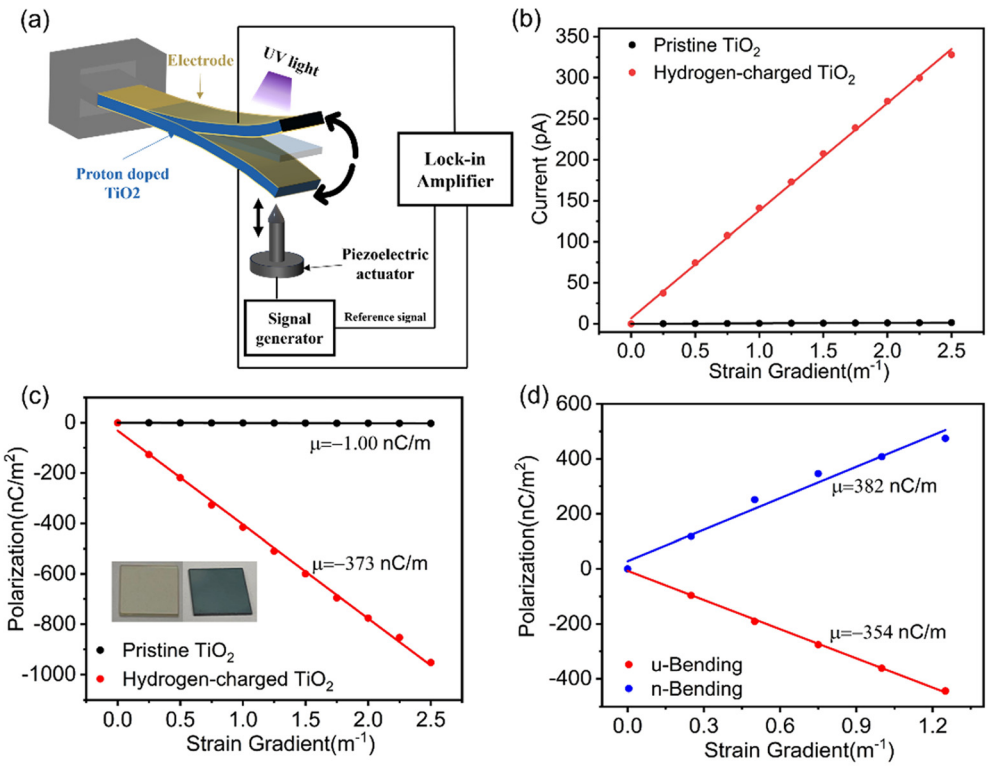

FIG. 2. (a) Schematic diagram of flexoelectric measurement setup showing the bending fixtures to introduce dynamic strain gradient to samples. (b) Original currents obtained by the lock-in amplifier for pristine TiO_2 and proton doped TiO_2 at different strain gradients. (c) Effective flexoelectric effect of pristine and proton doped TiO_2 crystals. (d) Comparison of the flexoelectric coefficients corresponding to n- and u-shaped bending for the proton doped TiO_2 crystal.

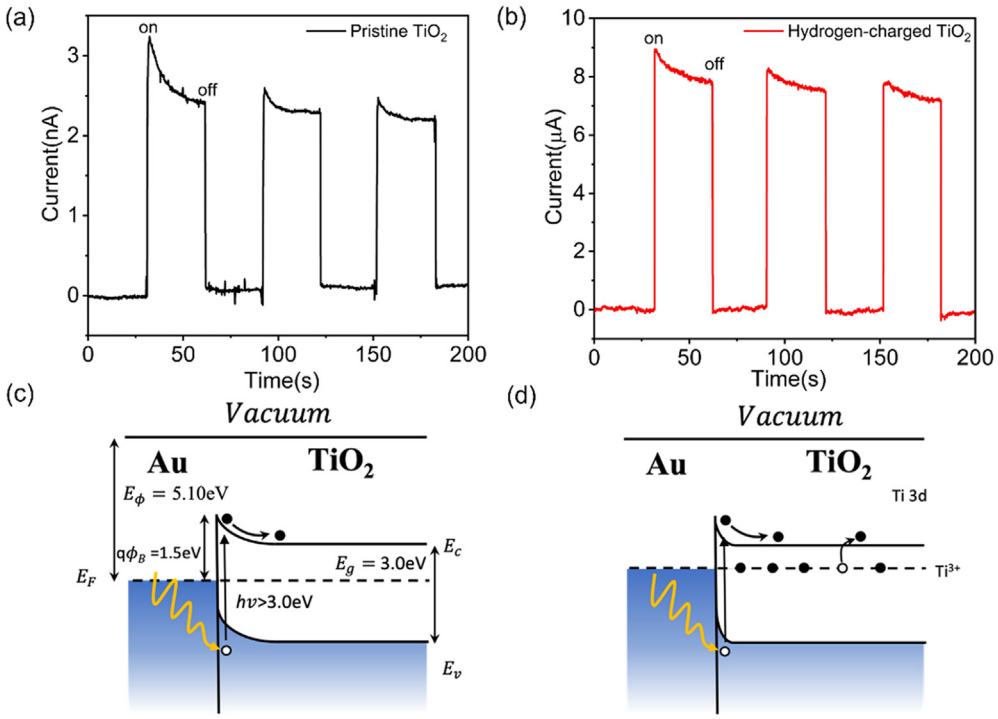

FIG. 3. (a) Photocurrent at the Au/TiO_2 interface for pristine, and (b) proton doped TiO_2 crystals. Energy band diagrams and electron tunneling at the Au/TiO_2 interface for pristine (c), and proton doped (d), TiO_2 crystals under UV light illumination. E_c is the energy conduction band minimum, E_v the energy valence band maximum, E_ϕ the work function, ϕ_B the barrier height, and E_g the bandgap.

useful for the development of memristors or photoelectric memristors for neuromorphic computing.

To prove the n-type conduction nature of the proton doped TiO_2 crystal, we also conducted the Seebeck coefficient and conductivity measurements, and the results are shown in Figs. 4(b) and 4(c). One can see that the hydrogen-charged TiO_2 crystal is an n-type semiconductor. The increase in the Seebeck coefficient and the decrease in the conductance in the second cycle of measurement are observed. We can observe that the blue color of the crystal became weaker after the measurement. The thermal powers of the crystal for the two-cycles of measurement are shown in Fig. 4(d), where one can see that the out-diffusion of proton also reduces the thermal power.

DFT calculation of 4% proton doped TiO_2 was also performed to understand the mechanism of increased flexoelectricity. Based on the simulation model, **a** is 4.77 Å (pristine 4.59 Å), **b** is 4.82 Å (pristine 4.59 Å), and **c** is 2.96Å (pristine 2.95 Å) for the 4% proton doped TiO_2. When the doping concentration increases to 14%, **a** is 4.84 Å, **b** is 4.85 Å, and **c** is 3.02Å. With proton doping, the lattice is distorted, and its unit cell expands in **a**, **b,** and **c** directions. Our calculated bandgap of pristine TiO_2 crystal is 2.3 eV. Even though the size of the unit cell increases slightly after doping, the computed bandgap value is reduced by approximately 10%–20%, as shown in Fig. 5(a). The preference of protons in TiO_2 is the site of its oxygen octahedral, this result is consistent with an earlier report,[63] and it is interesting to see that all protons point to the same direction after performing geometric optimization in the computational setup in Fig. 5(b). In the proton doped TiO_2 crystal, weak O–H bond is formed with a bond distance of d= 0.1 nm, and the formation of the O–H bond induces an electric polarization in its unit cells; the O–H bond distance of 0.1 nm creates an additional electric dipole of $\delta Q_+ \frac{d}{2} + \delta Q_- \frac{d}{2} = 2.16 \times 10^{-29}$ cm at each site, as shown in Fig. 5(c), where δQ is the variation in charges in O–H bond. Based on this dipole value of one O–H bond, if one unit cell is doped with one H, the polarization is in the same scale of $BaTiO_3$. Interestingly, when compared to pristine TiO_2, the dielectric constant of 4% proton doped TiO_2 and 14% proton doped TiO_2 is increased by 8.3 and 9.8 times, respectively. The bond angle of O–H may also be easily changed under strain gradient, giving rise to large flexoelectricity analogous to polarization switching induced flexoelectricity, where the schematic diagram is drawn in Fig. 5(d). A more detailed study in modeling needs to be carried out to understand the physics behind this interesting result.

According to the barrier layer model,[13,64] the photo-flexoelectric enhancement could be attributed to the narrowing of the depletion layer of the Schottky barrier at the Au/TiO_2 interface. In our experiment, induced protons can increase the charge carrier concentration in TiO_2 and further shrink the width of the depletion region. A quantitative dependence of the effective flexoelectric coefficient μ_{eff} of semiconducting materials is given by[15]

$$\mu_{\text{eff}} \equiv \sqrt{\frac{n\varepsilon_0\varepsilon_r}{2\phi_0}}\varphi\frac{t}{2}, \tag{1}$$

where n is the free carrier concentration, ε_0 is the vacuum dielectric permittivity, ε_r is the relative dielectric constant, ϕ_0 is the Schottky barrier height, φ is the surface deformation potential, and t is the sample

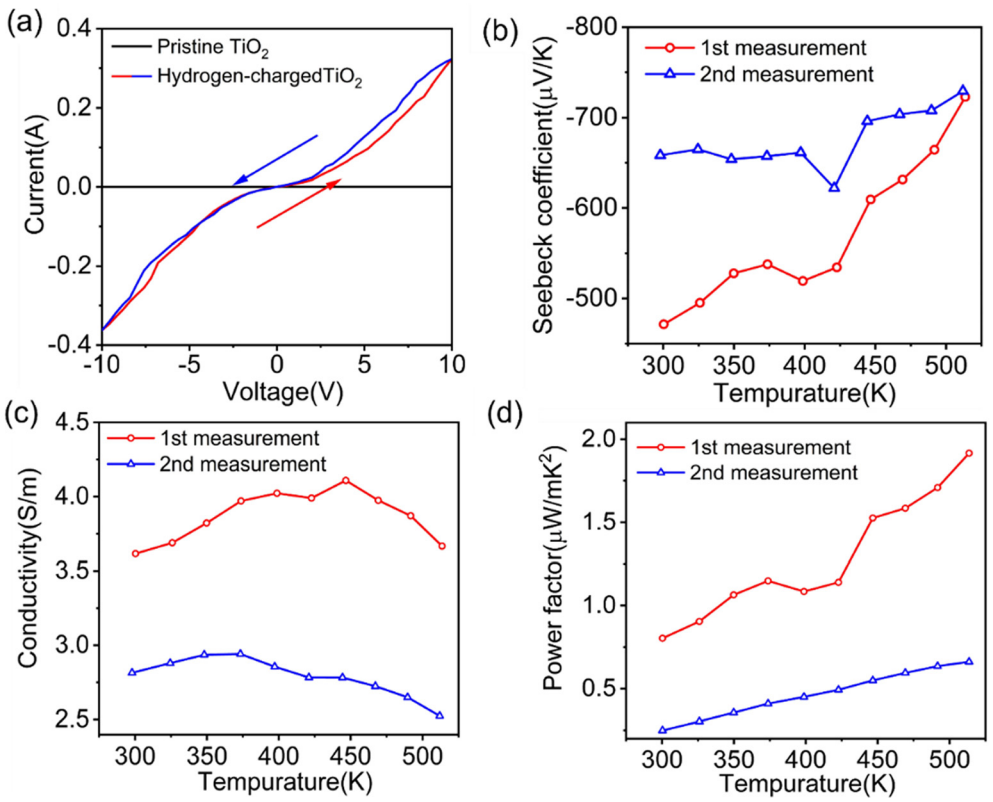

FIG. 4. (a) I–V curves of pristine (black line) and proton-charged (red line) TiO_2 crystals. (b) Temperature-dependent Seebeck coefficient, (c) electrical conductivity, and (d) thermal power, within the temperature range from 300 to 550 K.

thickness. The change in the free charge carrier concentration can be a major factor influencing the change in μ_{eff} in our experiment, while the flexoelectric enhancement observed in the reduced TiO_2 sample under dark conditions corresponds to two orders of magnitude increase in the free carrier concentration. As shown in Fig. 2(c), a much larger increment of μ_{eff} can be observed on the proton doped TiO_2 sample, and the presence of protons in the TiO_2 crystal can be attributed to the observed flexoelectric enhancement. These protons introduce defect levels, which effectively lower the Fermi level of TiO_2 and subsequently decrease the Schottky barrier height at the interface. As a result, the effective flexoelectric coefficient (μ_{eff}) in Eq. (1) is significantly increased. The significant increase in photocurrent for the proton doped sample in Fig. 3(b) is attributed to the doping-induced defect levels within the bandgap, which act as light absorption centers that convert photon energy into electron–hole pairs. On the other hand, when we bent the sample, we did not observe a clear enhancement of the photovoltaic effect because the contribution of the flexoelectric current to the charge transfer across the Schottky junction at the surface is much smaller compared to the photocurrent. As reported by Wang[51] and Zhai,[65] the formation of O–H vacancies (V_o) contributes to the reduction of bandgap, leading to an enhanced photovoltaic effect. The increase in the Seebeck coefficient and the decrease in the conductance in the second cycle of measurement [Figs. 4(b) and 4(c)] originate from the out-diffusion of protons from the crystal resulting in a decreased charge carrier density. Similarly, the pale blue color of the sample after the measurement can also be concluded that the out-diffusion of protons in the crystal reduced the charge carrier density, giving rise to increased Seebeck coefficient and reduced conductivity.

From the lattice distortion point of view, when protons are interstitially doped into oxide materials, they can create local strain fields within the crystal structure. These strain fields introduce gradients in the lattice parameters or atomic displacements, leading to variations in strain across the material. As a result, the flexoelectric effect is activated, causing the material to generate an electric polarization in response to the strain gradients under a large dielectric background. In the case of proton doping in TiO_2, the high charge density and high mobility of proton allow them to easily occupy interstitial lattice sites. By occupying these interstitial sites, proton atoms can perturb the local environment and introduce strain variations effective in inducing strain gradients, leading to strain variations on a nanoscale level. The production of a significant and enduring electric polarization is attributed not only to proton doping under strain variation but also to the substantial increase in dielectric constant, as depicted in Fig. 5(a). The decreased bandgap makes the TiO_2 crystal semiconducting with the presence of more charge carries contributing to the flexoelectric current; it is also called as flexoelectric-like by Catalan's group.[13]

With the help of BLYP functional, the calculated bandgap (2.3 eV) of pristine TiO_2 is much closer to the experimental value (3 eV), as plotted in Fig. 5(a). Figure S1 shows computed band structures of the pristine TiO_2 and proton doped TiO_2. However, our

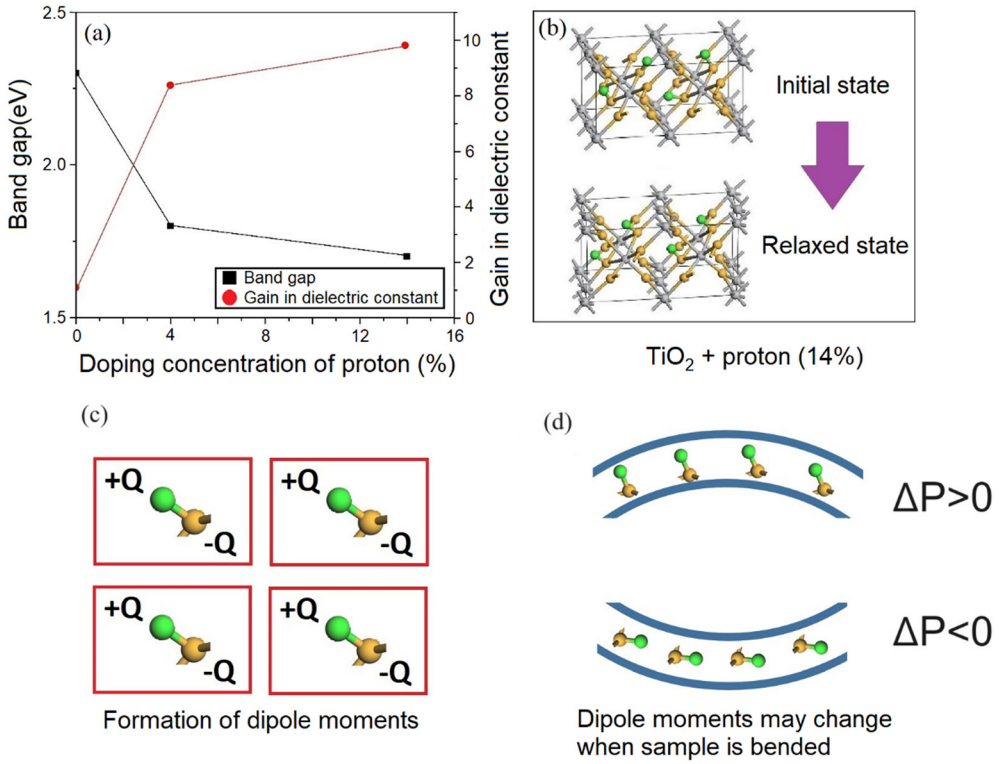

FIG. 5. (a) The computed bandgaps and dielectric constants of TiO_2 as a function of proton doping. (b) The schematic diagram of 14% proton doped TiO_2 crystal in DFT calculations. The repeating unit is shown. The Ti atoms, O atoms, and protons are marked by silver, yellow, and green colors, respectively. Removing three hydrogen atoms in (b) refers to 4% proton doped TiO_2 crystal. (c) The dipole moment between the O–H bond is formed by the separation of the electric charge $+Q$ and $-Q$. (d) The redistribution of dipole moment can be triggered by bending stress leading to the change of polarization, i.e., a contribution to flexoelectricity.

research objective is not focused on finding a perfect DFT functional for TiO_2. Instead, our main goal is to gain a deeper understanding of the impact of bandgap on proton doped TiO_2 crystals. For this purpose, it is fair enough to employ a reasonable and well-established DFT functional BYLP to compare the bandgap of TiO_2 with and without proton doping. Contrary to expectations, the bandgap of TiO_2 does not increase when proton dopants expand the lattice. This unexpected observation may be attributed to the induced electric polarization, which leads to an increase in charge fluctuation. As a result, there is an increase in the overlap of wavefunctions in the proton doped TiO_2 to increase electric conductivity. By increasing the concentration of proton in TiO_2 in the simulator, the bandgap value will decrease even further with the evidence in Fig. 5(a).

In comparison to the generally small magnitude of the intrinsic flexoelectric effect in oxide materials, non-intrinsic flexoelectricity induced by dopants has the potential to exhibit a significant increase by orders of magnitude. Compared to vacuum annealing induced oxygen vacancy and reduction of the cations (such as Ti^{4+} changes to Ti^{3+}), this work demonstrates a promising approach of proton doping in insulating oxide materials, leading to robust flexoelectricity. Highly insulated oxide can generate flexoelectric field but with very low flexoelectric current. The increased charge carries in the proton doped oxide contributes more flexoelectric current driven by the flexoelectric field. In our control experiment, annealed TiO_2 does not show any increase in flexoelectricity (see Fig. S2). We believe that for a specific oxide material, there should be an optimized charge carrier density resulting in the maximum flexoelectricity when considering the quantitative correlation between the flexoelectric coefficient and charge carrier density. However, when the doped material turns from a semiconducting state to a metallic state, the flexoelectric field will be screened by free electrons, leading to zero-flexoelectricity. A more detailed quantitative study deserves further study.

In conclusion, the proton doping effect on flexoelectricity of TiO_2 crystal has been studied. It is found that by introducing protons in TiO_2, the effective flexoelectric coefficient can be enhanced by over two orders of magnitude, and its photovoltaic effect can be increased by three orders of magnitude. These results help understand the mechanism of exotic flexoelectricity and may also provide application of the giant flexoelectric effect in energy conversion applications such as energy harvester and accelerometers, etc.

See the supplementary material for Figure S1, which shows the band structure of TiO_2 as a function of doping level, and Figure S2, which shows the control results of the flexural electrical experiments on thermally annealed TiO_2 single crystals.

This work was supported by the Hong Kong Research Grants Council (Grant No. 15301421) and the National Natural Science Foundation of China (Grants Nos. 11674031, 11474022, and 12104250).

AUTHOR DECLARATIONS

Conflict of Interest

The authors have no conflicts to disclose.

Author Contributions

Zelong Wang and Yangshi Jin contributed equally to this work.

Zelong Wang: Data curation (lead). **Wan Ping Chen:** Data curation (equal); Supervision (equal). **Xiaoyuan Zhou:** Data curation (equal). **Jiyan Dai:** Supervision (lead); Writing – review & editing (lead). **Yangshi Jin:** Data curation (lead). **Chun Hung Suen:** Data curation (supporting). **Chenyue Mao:** Data curation (equal). **Xiangnan Gong:** Data curation (supporting). **Jiangping Ma:** Data curation (supporting). **Jiawang Hong:** Data curation (supporting). **Fan Zhang:** Data curation (supporting). **Chi Ho Wong:** Formal analysis (lead); Writing – original draft (equal).

DATA AVAILABILITY

The data that support the findings of this study are available from the corresponding author upon reasonable request.

REFERENCES

[1]X. Yan, W. Huang, S. Ryung Kwon, S. Yang, X. Jiang, and F.-G. Yuan, "A sensor for the direct measurement of curvature based on flexoelectricity," Smart Mater. Struct. **22**(8), 085016 (2013).

[2]M.-M. Yang, D. J. Kim, and M. Alexe, "Flexo-photovoltaic effect," Science **360**(6391), 904–907 (2018).

[3]F. J. Maier, M. Schneider, J. Schrattenholzer, W. Artner, K. Hradil, A. Artemenko, A. Kromka, and U. Schmid, "Flexoelectricity in polycrystalline TiO_2 thin films," Acta Mater. **190**, 124–129 (2020).

[4]X. Chen, X. Tang, X.-Z. Chen, Y.-L. Chen, X. Guo, H.-X. Ge, and Q.-D. Shen, "Nonvolatile data storage using mechanical force-induced polarization switching in ferroelectric polymer," Appl. Phys. Lett. **106**(4), 042903 (2015).

[5]R. A. Surmenev and M. A. Surmeneva, "The influence of the flexoelectric effect on materials properties with the emphasis on photovoltaic and related applications: A review," Mater. Today **67**, 256 (2023).

[6]L. Liu, "An energy formulation of continuum magneto-electro-elasticity with applications," J. Mech. Phys. Solids **63**, 451–480 (2014).

[7]W. Ma and L. E. Cross, "Flexoelectric effect in ceramic lead zirconate titanate," Appl. Phys. Lett. **86**(7), 072905 (2005).

[8]P. Zubko, G. Catalan, and A. K. Tagantsev, "Flexoelectric effect in solids," Annu. Rev. Mater. Res. **43**(1), 387–421 (2013).

[9]L. Wang, S. Liu, X. Feng, C. Zhang, L. Zhu, J. Zhai, Y. Qin, and Z. L. Wang, "Flexoelectronics of centrosymmetric semiconductors," Nat. Nanotechnol. **15**(8), 661–667 (2020).

[10]F. Zhang, P. Lv, Y. Zhang, S. Huang, C.-M. Wong, H.-M. Yau, X. Chen, Z. Wen, X. Jiang, C. Zeng, J. Hong, and J-y Dai, "Modulating the electrical transport in the two-dimensional electron gas at $LaAlO_3/SrTiO_3$ heterostructures by interfacial flexoelectricity," Phys. Rev. Lett. **122**, 257601 (2019).

[11]A. K. Tagantsev, "Piezoelectricity and flexoelectricity in crystalline dielectrics," Phys. Rev. B **34**(8), 5883–5889 (1986).

[12]S. Mao and P. K. Purohit, "Defects in flexoelectric solids," J. Mech. Phys. Solids **84**, 95–115 (2015).

[13]J. Narvaez, F. Vasquez-Sancho, and G. Catalan, "Enhanced flexoelectric-like response in oxide semiconductors," Nature **538**(7624), 219–221 (2016).

[14]L. Shu, M. Wan, Z. Wang, L. Wang, S. Lei, T. Wang, W. Huang, N. Zhou, and Y. Wang, "Large flexoelectricity in Al_2O_3-doped $Ba(Ti_{0.85}Sn_{0.15})O_3$ ceramics," Appl. Phys. Lett. **110**(19), 192903 (2017).

[15]L. Shu, S. Ke, L. Fei, W. Huang, Z. Wang, J. Gong, X. Jiang, L. Wang, F. Li, S. Lei, Z. Rao, Y. Zhou, R.-K. Zheng, X. Yao, Y. Wang, M. Stengel, and G. Catalan, "Photoflexoelectric effect in halide perovskites," Nat. Mater. **19**(6), 605–609 (2020).

[16]F. Zhang, W.-M. Jiang, C.-J. Li, Y. Jin, Z. Wang, J.-C. Nie, and J. Dai, "Flexoelectric modulation on the two-dimensional electron gas at (110) $LaAlO_3/SrTiO_3$ interfaces," ACS Appl. Electron. Mater. **2**, 1861–1866 (2020).

[17]J. Mannhart and D. G. Schlom, "Oxide interfaces—An opportunity for electronics," Science **327**, 1607–1611 (2010).

[18]Y. Jin, F. Zhang, K. Zhou, C. H. Suen, X. Y. Zhou, and J.-Y. Dai, "Oxygen vacancy and photoelectron enhanced flexoelectricity in perovskite $SrTiO_3$ crystal," Appl. Phys. Lett. **118**, 164101 (2021).

[19]J. Hwang, Z. Feng, N. Charles, X. R. Wang, D. Lee, K. A. Stoerzinger, S. Muy, R. R. Rao, D. Lee, R. Jacobs, and D. Morgan, "Tuning perovskite oxides by strain: Electronic structure, properties, and functions in (electro) catalysis and ferroelectricity," Mater. Today **31**, 100–118 (2019).

[20]L. Ma, J. Wu, T. Zhu, Y. Huang, Q. Lu, and S. Liu, "Ultrahigh oxygen ion mobility in ferroelectric Hafnia," Phys. Rev. Lett. **131**, 256801 (2023).

[21]K. Cordero-Edwards, N. Domingo, A. Abdollahi, J. Sort, and G. Catalan, "Ferroelectrics as smart mechanical materials," Adv. Mater. **29**(37), 1702210 (2017).

[22]U. K. Bhaskar, N. Banerjee, A. Abdollahi, E. Solanas, G. Rijnders, and G. Catalan, "Flexoelectric MEMS: Towards an electromechanical strain diode," Nanoscale **8**(3), 1293–1298 (2016).

[23]K. Cordero-Edwards, H. Kianirad, C. Canalias, J. Sort, and G. Catalan, "Flexoelectric fracture-ratchet effect in ferroelectrics," Phys. Rev. Lett. **122**(13), 135502 (2019).

[24]Q. Huang, Z. Fan, J. Rao, T. Yang, X. Zhang, D. Chen, M. Qin, M. Zeng, X. Lu, G. Zhou, and X. Gao, "Significant modulation of ferroelectric photovoltaic behavior by a giant macroscopic flexoelectric effect induced by strain-relaxed epitaxy," Adv. Electron. Mater. **8**(1), 2100612 (2022).

[25]L. Han, X. Yang, Y. Lun, Y. Guan, F. Huang, S. Wang, J. Yang, C. Gu, Z. B. Gu, L. Liu, and Y. Wang, "Tuning piezoelectricity via thermal annealing at a free-standing ferroelectric membrane," Nano Lett. **23**(7), 2808–2815 (2023).

[26]J. Xu, W. Zheng, Y. Yu, C. Ding, M. Wu, and Z. Wen, "Effects of flexoelectric polarization on surface potential of dielectric thin-film heterostructures: A comparative study," Appl. Phys. Lett. **121**(20), 203502 (2022).

[27]S. Cai, Y. Lun, D. Ji, P. Lv, L. Han, C. Guo, Y. Zang, S. Gao, Y. Wei, M. Gu, and C. Zhang, "Enhanced polarization and abnormal flexural deformation in bent freestanding perovskite oxides," Nat. Commun. **13**(1), 5116 (2022).

[28]F. Yu, J. Tian, F. Jiang, Y. Liu, C. Li, C. Wang, Z. L. Wang, and K. Ren, "Flexoelectricity-enhanced photovoltaic effect in trapezoid-shaped $NaNbO_3$ nanotube array composites," Nano Res. **16**(9), 11914–11924 (2023).

[29]D. Yan, J. Wang, J. Xiang, Y. Xing, and L. H. Shao, "A flexoelectricity-enabled ultrahigh piezoelectric effect of a polymeric composite foam as a strain-gradient electric generator," Sci. Adv. **9**(2), eadc8845 (2023).

[30]H. L. Dai, Z. Yan, and L. Wang, "Nonlinear analysis of flexoelectric energy harvesters under force excitations," Int. J. Mech. Mater. Des. **16**, 19–33 (2020).

[31]J. W. Zhang and Z. H. Lai, "Numerical investigation on a bistable vibro-impact dielectric elastomer generator mounted on a vibrating structure with ultra-low natural frequency," Int. J. Mech. Mater. Des. **19**, 687 (2023).

[32]Z. Yan, "Modeling of a piezoelectric/piezomagnetic nano energy harvester based on two dimensional theory," Smart Mater. Struct. **27**(1), 015016 (2017).

[33]L. Qi, S. Huang, G. Fu, S. Zhou, and X. Jiang, "On the mechanics of curved flexoelectric microbeams," Int. J. Eng. Sci. **124**, 1–15 (2018).

[34]R. Guo, L. You, W. Lin, A. Abdelsamie, X. Shu, G. Zhou, S. Chen, L. Liu, X. Yan, J. Wang, and J. Chen, "Continuously controllable photoconductance in freestanding $BiFeO_3$ by the macroscopic flexoelectric effect," Nat. Commun. **11**(1), 2571 (2020).

[35]P. Jiao, H. Cheng, J. Li, H. Chen, Z. Liu, Z. Xi, W. Ding, X. Ma, J. Wang, N. Zheng, and Y. Nie, "Flexoelectricity-stabilized ferroelectric phase with enhanced reliability in ultrathin La:HfO_2 films," Appl. Phys. Rev. **10**, 031417 (2023).

[36]M. Wu, Z. Jiang, X. Lou, F. Zhang, D. Song, S. Ning, M. Guo, S. J. Pennycook, J. Y. Dai, and Z. Wen, "Flexoelectric thin-film photodetectors," Nano Lett. **21**(7), 2946–2952 (2021).

[37]Y. Su, X. Lin, R. Huang, and Z. Zhou, "Analytical electromechanical modeling of nanoscale flexoelectric energy harvesting," Appl. Sci. **9**(11), 2273 (2019).

[38]H. Tan, W. Si, W. Peng, X. Chen, X. Liu, Y. You, L. Wang, F. Hou, and J. Liang, "Flexo-/piezoelectric polarization boosting exciton dissociation in curved two-dimensional carbon nitride photocatalyst," Nano Lett. **23**(22), 10571–10578 (2023).

[39]L. Zhu, R. Liang, M. Ye, L. Shu, R. Zheng, and S. Ke, "Thickness-dependent flexoresistance in $SrTiO_3$ thin films," Appl. Phys. Lett. **122**(16), 162901 (2023).
[40]W. Yang, Q. Deng, X. Liang, and S. Shen, "Lamb wave propagation with flexoelectricity and strain gradient elasticity considered," Smart Mater. Struct. **27**(8), 085003 (2018).
[41]H. Sun, J. Gu, Y. Li, T. R. Paudel, D. Liu, J. Wang, Y. Zang, C. Gu, J. Yang, W. Sun, and Z. Gu, "Prominent size effects without a depolarization field observed in ultrathin ferroelectric oxide membranes," Phys. Rev. Lett. **130**(12), 126801 (2023).
[42]H. Lu, C. W. Bark, D. Esque De Los Ojos, J. Alcala, C. B. Eom, G. Catalan, and A. Gruverman, "Mechanical writing of ferroelectric polarization," Science **336**(6077), 59–61 (2012).
[43]J.-H. Ahn, P. C. McIntyre, L. W. Mirkarimi, S. R. Gilbert, J. Amano, and M. Schulberg, "Deuterium-induced degradation of (Ba, Sr,)TiO_3 films," Appl. Phys. Lett. **77**(9), 1378–1380 (2000).
[44]S. Aggarwal, S. R. Perusse, C. W. Tipton, R. Ramesh, H. D. Drew, T. Venkatesan, D. B. Romero, V. B. Podobedov, and A. Weber, "Effect of hydrogen on Pb(Zr,Ti)O_3-based ferroelectric capacitors," Appl. Phys. Lett. **73**(14), 1973–1975 (1998).
[45]N. Poonawala, V. P. Dravid, O. Auciello, J. Im, and A. R. Krauss, "Transmission electron microscopy study of hydrogen-induced degradation in strontium bismuth tantalate thin films," J. Appl. Phys. **87**(5), 2227–2231 (2000).
[46]P. F. Chester and D. H. Bradhurst, "Electrolytically induced conductivity in rutile," Nature **199**, 1056–1057 (1963).
[47]W. P. Chen, K. F. He, Y. Wang, H. L. W. Chan, and Z. Yan, "Highly mobile and reactive state of hydrogen in metal oxide semiconductors at room temperature," Sci. Rep. **3**, 3149 (2013).
[48]L.-B. Mo, Y. Wang, Y. Bai, Q.-Y. Xiang, and Q. Li, "Hydrogen impurity defects in rutile TiO_2," Sci. Rep. **5**, 17634 (2015).
[49]J. Herbert, *Ceramic Dielectrics and Capacitors* (CRC Press, 1985), Vol. 6.
[50]X. Chen, L. Liu, P. Y. Yu, and S. S. Mao, "Increasing solar absorption for photocatalysis with black hydrogenated titanium dioxide nanocrystals," Science **331**(6018), 746–750 (2011).
[51]G. Wang, H. Wang, Y. Ling, Y. Tang, X. Yang, R. C. Fitzmorris, C. Wang, J. Z. Zhang, and Y. Li, "Hydrogen-treated TiO_2 nanowire arrays for photoelectrochemical water splitting," Nano Lett. **11**(7), 3026–3033 (2011).
[52]F. Herklotz, E. V. Lavrov, and J. Weber, "Infrared absorption of the hydrogen donor in rutile TiO_2," Phys. Rev. B **83**(23), 235202 (2011).
[53]C. Kılıç and A. Zunger, "n-type doping of oxides by hydrogen," Appl. Phys. Lett. **81**, 73–75 (2002).
[54]A. Naldoni, M. Allieta, S. Santangelo, M. Marelli, and F. Fabbri, "Effect of nature and location of defects on bandgap narrowing in black TiO_2 nanoparticles," J. Am. Chem. Soc. **134**, 7600–7603 (2012).
[55]L. Liu, P. Y. Yu, X. Chen, S. S. Mao, and D. Z. Shen, "Hydrogenation and disorder in engineered black TiO_2," Phys. Rev. Lett. **111**, 065505 (2013).
[56]L. Zhang, Z. Wang, S. Shu, Y. Hu, C. Li, S. Ke, F. Li, and L. Shu, "Origin of defects induced large flexoelectricity in ferroelectric ceramics," Phys. Rev. Mater. **6**(9), 094416 (2022).
[57]Z. Dai, S. Guo, Y. Gong, and Z. Wang, "Semiconductor flexoelectricity in graphite-doped $SrTiO_3$ ceramics," Ceram. Int. **47**(5), 6535–6539 (2021).
[58]Y. Li, L. Shu, Y. Zhou, J. Guo, F. Xiang, L. He, and H. Wang, "Enhanced flexoelectric effect in a non-ferroelectric composite," Appl. Phys. Lett. **103**(14), 142909 (2013).
[59]P. Zubko, G. Catalan, A. Buckley, P. R. L. Welche, and J. F. Scott, "Strain-gradient-induced polarization in $SrTiO_3$ single crystals," Phys. Rev. Lett. **99**(16), 167601 (2007).
[60]P. A. Baldi, M. P. De Micheli, K. E. Hadi, S. Nouh, A. C. Cino, P. Aschieri, and D. B. Ostrowsky, "Proton exchanged waveguides in $LiNbO_3$ and $LiTaO_3$ for integrated lasers and nonlinear frequency converters," Opt. Eng. **37**(4), 1193–1202 (1998).
[61]Z. Chen, W. Li, Z. Fan, S. Dong, Y. Chen, M. Qin, M. Zeng, X. Lu, G. Zhou, X. Gao, and J.-M. Liu, "All-ferroelectric implementation of reservoir computing," Nat. Commun. **14**(1), 3585 (2023).
[62]B. Cui, Z. Fan, W. Li, Y. Chen, S. Dong, Z. Tan, S. Cheng, B. Tian, R. Tao, G. Tian, D. Chen, Z. Hou, M. Qin, M. Zeng, X. Lu, G. Zhou, X. Gao, and J.-M. Liu, "Ferroelectric photosensor network: An advanced hardware solution to real-time machine vision," Nat. Commun. **13**(1), 1707 (2022).
[63]M. V. Koudriachova, S. W. De Leeuw, and N. M. Harrison, "First-principles study of H intercalation in rutile TiO_2," Phys. Rev. B **70**(16), 165421 (2004).
[64]D. O'Neill, R. M. Bowman, and J. M. Gregg, "Dielectric enhancement and Maxwell–Wagner effects in ferroelectric superlattice structures," Appl. Phys. Lett. **77**(10), 1520–1522 (2000).
[65]T. Zhai, S. Xie, M. Yu, P. Fang, C. Liang, X. Lu, and Y. Tong, "Oxygen vacancies enhancing capacitive properties of MnO_2 nanorods for wearable asymmetric supercapacitors," Nano Energy **8**, 255–263 (2014).